



The Nanoaquarium: A New Paradigm in Electron Microscopy

Joseph M. Grogan¹, Nicholas M. Schneider¹, Frances M. Ross² and Haim H. Bau¹

Abstract | Since its invention, the electron microscope has facilitated numerous advances in a plethora of disciplines ranging from materials science, physics, and chemistry, to biology. Traditional electron microscopy must be carried out, however, in a high vacuum environment that does not allow for real time imaging of processes in liquid media. Consequently, traditional electron microscopy has been restricted to painstaking “*postmortem*” investigations on dry or frozen samples without any guarantee that an image is captured at the “*right*” moment. Static images also do not provide information on process dynamics, and the sample preparation may adversely impact the structure of the object to be imaged. The ability to image dynamic processes in liquid media is certain to be transformative, lead to new discoveries, and provide a better understanding of many important processes at the nanoscale. To overcome the limitations of traditional electron microscopy, there has been a growing interest in recent years in developing means for wet electron microscopy that will allow one to image samples in real time in their native environment and observe processes *in situ* as they take place. We briefly survey recent efforts pertaining to wet electron microscopy and then describe in greater detail the work of our group with a custom-made, micro-fabricated liquid cell dubbed the “nanoaquarium”. The nanoaquarium sandwiches a thin liquid layer, ranging in thickness from tens of nanometers to a few microns, between two thin, electron-transparent, silicon nitride membranes. The liquid cell is hermetically sealed from the vacuum environment of the electron microscope. The thin liquid layer scatters only a small fraction of the electrons and allows one to image objects suspended in the liquid with high resolution. We describe briefly the imaging of oriented assembly of colloidal crystals, diffusion limited aggregation of nanoparticles, and electrochemical processes.

1 Introduction

The invention of the electron microscope has facilitated numerous advances in many scientific fields such as materials science, chemistry, physics, biology, and medicine. The resolution of conventional light microscopy is limited by diffraction to about half the wavelength of light, which allows one to image features down to approximately 200 nm.

Electrons have a wavelength about 100,000 times shorter than visible light (photons). Thus, the electron microscope allows us to “see” sub-nm size features. Recently, researchers have reported electron microscope images with a resolution better than 50 pm (0.5 angstrom or 5×10^{-11} m).¹ The idea of imaging with electrons is credited to the physicist Leo Szilard, who filed for a patent for

¹Department of Mechanical Engineering and Applied Mechanics, University of Pennsylvania, Philadelphia, PA 19104-6315, USA.

²IBM T. J. Watson Research Center, Yorktown Heights, NY 10598, USA.

his invention.² The first electron microscope was constructed, however, by Ernst Ruska and Max Knoll in 1931.³ Ruska received the Nobel Prize in Physics in 1986 for his work on electron optics and for the design of the first electron microscope.

Since its inception in the 1930's, the transmission electron microscope (TEM), and later the scanning transmission electron microscope (STEM), have provided a powerful means to image features at the nanoscale. In addition to high resolution imaging, the TEM and STEM allow for material characterization, due to the unique interactions between the electron beam and the sample. These interactions provide qualitative information such as the relative densities and distribution of the various constituents in an inhomogeneous sample. They also provide precise elemental analysis through characteristic electron scattering (**electron energy loss spectroscopy**) and characteristic X-ray emission (**energy dispersive X-ray spectroscopy**). For these reasons, the TEM and STEM have become standard analytical tools in both the physical and the biological sciences. The electron microscope, however, must typically operate at a high vacuum to avoid scattering and absorption of electrons by the medium. This limits one to imaging solid materials or specially prepared, dried samples.

There are, though, many branches of science and technology that would benefit from the ability to observe dynamical processes in fluids in real time with nanoscale resolution. Examples include nanoscale phenomena such as nanoparticle interactions; formation of colloidal crystals with unique optical and electrical properties (metamaterials); electrochemical deposition and etching; nucleation and growth of crystals and bubbles; processes associated with charging and discharging of batteries; interfacial phenomena; and biological interactions. Better understanding of the physics involved in such diverse phenomena will doubtlessly lead to new insights and the design of new and more effective processes and materials.

In the introduction to his widely cited article, "Wetting: statics and dynamics," the Nobel Prize winner P. G. de Gennes remarks that our understanding of phenomena at the liquid-solid interface is limited because "solid/liquid interfaces are much harder to probe than their solid/vacuum counterpart; essentially all experiments making use of electron beams become inapplicable when a fluid is present".⁴ The difficulty that de Gennes refers to is the fact that standard electron microscopes operate at high vacuum, and so most liquid samples, particularly aqueous solutions, will quickly evaporate in this environment and will not

be accessible for observations. Water at 25°C will boil at an approximate pressure of 24 Torr,⁵ which is much higher than a typical (S)TEM chamber's pressure. Additionally, in order to provide reasonable resolution and contrast between suspended objects and the suspending medium in all imaging modes (bright field, dark field, and high angle annular dark field), one must use very thin slices of sample (i.e. liquid) to avoid excessive scattering and absorption of electrons. Typically, to study a process occurring in liquid media, one must fix (freeze or dry out) samples at various stages of the process and carry out *ex situ* imaging. Although this procedure has resulted in major advances in disciplines ranging from materials science to biology, it suffers from some limitations. Imaging of fixed samples does not capture the dynamics of a process; only static snapshots are captured during the process. Moreover, it is difficult to select the "right" moment to fix the sample, so critical observations may be lost. Also, the sample preparation process for electron imaging may alter the sample in fundamental ways. Thus, researchers have sought to address the challenges of liquid imaging in the electron microscope through various approaches.

2 Brief Review of Wet Electron Microscopy

Several different techniques for imaging liquids in the electron microscope have been summarized recently.⁶ Generally, wet electron microscopy can be separated into two main categories: open liquid cells and closed liquid cells. In the case of the open liquid cell, the liquid is exposed to the vacuum environment of the microscope through an aperture and the state of the liquid is dynamic. In the case of the closed cell, the liquid is hermetically sealed and does not evaporate.

2.1 Open liquid cell

In the case of the open liquid cell, the liquid sample is contained in a vessel that allows passage of the electron beam through a small hole in the top, known as the pressure-limiting aperture, while minimizing loss of vapor to the high vacuum environment outside the vessel. The aperture allows the electron source/gun to remain at high vacuum while the vessel is at low vacuum or near-atmospheric pressure. The vessel can be a **micro or meso-fabricated** device that is inserted into the imaging chamber with little or no modification to the microscope. A second aperture can be placed on the bottom side of the vessel to allow TEM imaging of the liquid sample contained within. Alternatively, the microscope itself can be modified with a series of differentially pumped chambers along the

Electron energy loss spectroscopy: Inelastic scattering is an electron-electron interaction between the incident beam and the sample that causes the incident electron to lose some energy (ΔE). The energy loss spectrum of the incident electron can be analyzed to obtain information about the electronic structure and chemical composition of the sample.

Energy dispersive X-ray spectroscopy: When an incident electron transfers some energy to a sample (ΔE) it causes atoms in the sample to enter an excited state or release a secondary electron through ionization. The vacancy left by an excited or ionized electron is filled by an electron from a higher state and the energy difference may be emitted as an X-ray. The characteristics of the emitted X-ray are unique to every element and can be analyzed to obtain information about the elemental composition of the sample.

Micro or meso-fabricated: A micro-fabricated device contains features on the micrometer scale and typically involved MEMS or semiconductor manufacturing techniques such as photolithography, thin film deposition, etching, and the like. A meso-fabricated device loosely describes a device containing features between the micrometer and millimeter length scale and would typically require precision machining, though not clean-room facilities.

beam column, separated by apertures, that turns the entire imaging chamber into the sample storage vessel. In this case, the vessel is large enough to accommodate specially designed detectors to allow SEM imaging of the liquid sample. In either case, the vapor leaking from the specimen vessel is removed by the pumping system before it can reach the electron gun. This is the principle behind instruments such as the environmental transmission electron microscope (ETEM) and the environmental scanning electron microscope (ESEM).

Typically, ETEM is used for *in situ* studies in gaseous rather than liquid environments. ESEM is a powerful technique for imaging hydrated solid samples (e.g., imaging the surface structure of biological material without the need for sample preparation/modification/fixing). It also provides benefits when imaging samples prone to charging problems such as dielectric surfaces. The interaction of the electron beam with the water vapor produces a cascade effect that amplifies the signal to the **gaseous secondary electron detector (GSED)**, allows imaging of non-conducting samples, and mitigates charge buildup effects.⁷

The ESEM aperture approach, however, has its drawbacks when it comes to imaging of liquids. While the evaporation issue is alleviated with the use of apertures, it is not eliminated; and continuous evaporation and condensation make it difficult to precisely control the thickness of the liquid layer. Care must be taken with the vapor pressure in the ESEM chamber to ensure favorable imaging conditions while also ensuring that the sample does not dry out. Most importantly, in ESEM, only the top layer of the liquid sample is imaged, with minimal penetration of the beam into the liquid.⁸ Observations are thus mostly limited to the portion of the sample at the liquid-vapor interface (top of the drop), and one is prevented from imaging processes inside the liquid volume or, in the case of a droplet, the part that is in contact with the solid substrate. Additionally, one must either purchase an ESEM capable microscope or perform significant modifications to a standard SEM to enable ESEM capabilities.

2.2 Closed liquid cell

To overcome the shortcomings of the environmental electron microscope, researchers have developed closed liquid cells or liquid capsules that hermetically seal the liquid, preventing evaporation while the microscope chamber is maintained at a high vacuum. For example, Quantomix has pioneered a sealed, liquid-filled capsule capped with a 250 μm thick polymer (KaptonTM) membrane for imaging biological cells attached

to the membrane's underside.^{9–13} The capsule can be imaged only with backscattered electrons, providing limited resolution (~ 20 nm) and allowing only imaging of processes in close proximity to the membrane. Krueger et al. have recently modified the liquid capsule and replaced the polyimide membrane with a **graphene** membrane for improved imaging performance.¹⁴

In more recent devices, the liquid sample is contained in a thin vessel with two thin electron-transparent membranes serving as the “ceiling” and “floor” to prevent evaporation while allowing the electron beam to pass through the sample to produce an image. Devices that employ the encapsulation approach are referred to as liquid-cell (S)TEM devices. Liquid-cell devices sometimes require custom-fabricated sample holders; however, like the liquid capsule, they do not require any modifications to the microscope and they make it possible to view processes taking place in liquid media with a standard (S)TEM. To form a liquid slice that is sufficiently thin to minimize electron scattering by the suspending medium, researchers have relied on microfabrication technology. The various liquid-cell devices rely on the common theme of thin membranes separated by a spacer material to form a (hopefully) hermetically sealed chamber.^{14–31}

The details of each device differ in the choice of membrane material, sealing method, and spacer material. The spacer material dictates the distance between the membranes and the nominal height of the liquid cell. Unfortunately, in most cases, when the liquid cell is inserted into the vacuum chamber of the electron microscope, the difference between the pressure inside the cell and the outside pressure of the microscope's chamber will cause the very thin membranes to deform a great deal, resulting in a shape similar to a convex lens. The bowed out membranes thereby increase the effective thickness of the liquid layer well above the nominal, intended value.

Williamson et al.¹⁵ and Radisic et al.^{16,17} used 100 nm stoichiometric silicon nitride membranes with a 0.5–1 μm silicon oxide layer as the spacer and sealed the device with epoxy. Their device was used in a TEM to study electrochemical nucleation and growth of copper nanoclusters. Liu et al.¹⁸ used 9 nm silicon oxide membranes with a 2–5 μm epoxy spacer that also served to seal the device. Their device was used in a TEM to study live *E. coli* and *K. pneumoniae* cells and monitor biological processes. De Jonge et al.¹⁹ used 50 nm, low stress, silicon nitride membranes with 10 μm polystyrene microspheres as the spacer and sealed the device with a custom-made sample holder. Their device was used in a STEM

Graphene: A one atom thick planar sheet of carbon atoms in a honeycomb pattern. The drop casting method employed by Krueger et al. resulted in a thin membrane composed of many overlapping graphene sheets.

Gaseous secondary electron detector: The traditional SEM detector (ET type) cannot be used in an ESEM because the high voltage potential at which it operates can result in arcing in the gaseous environment. Whereas the traditional SEM detector is typically placed off axis from the beam path, the gaseous secondary electron detector of the ESEM is placed close to the beam path (often in the form of a disc directly in the beam path with a hole in the center that also serves as a pressure limiting aperture) in close physical proximity to the sample, and operates at lower potential. Secondary and backscattered electrons emitted from the sample ionize the gas molecules in the chamber and result in signal amplification to the detector via cascade collisions through the gas.

to study fibroblast cells with embedded, functionalized gold labels to track intracellular processes. De Jonge's group has since published several other studies addressing various aspects of liquid cell electron microscopy.^{20–22} Zheng et al.^{23,24} used 25 nm, low stress, silicon nitride membranes with a 200 nm indium layer as the spacer and sealing material. Their device was used in a TEM to study platinum nanocrystal growth and the diffusion of gold nanocrystals. The indium spacer provided, however, an imperfect seal, which allowed for slow evaporation of the liquid from the device. White et al.²⁵ used a silicon oxide/silicon nitride stack with thickness less than 50 nm as the membrane material with a 300 nm gold-palladium layer as the spacer, and sealed the device with epoxy. Their device was used in a TEM to study bubble formation due to Joule heating of a nanowire in water. Similar to the liquid cells, Creemer et al.²⁶ constructed a *gas* flow cell using a 4 μm thick, silicon oxide layer as the spacer and sealed the device with epoxy. Observation windows were formed in 1.2 μm thick, low stress, silicon nitride membranes by locally thinning the membrane down to 10 nm. Since the gas has much lower density than liquids, it was possible to operate with relatively tall devices. The device was used for TEM

imaging of copper nanocrystal growth at elevated temperatures in a hydrogen atmosphere. More recently, the group improved their original design and, like us, has employed wafer level processing throughout the fabrication process of their devices.^{27,28}

Additionally, commercial liquid-cell systems have recently been introduced by companies such as Hummingbird ScientificTM and ProtochipsTM. Typically, these systems use low stress, silicon nitride membranes (10s to 100s of nm thick) with a polymer spacer of some kind (beads or photopatterned epoxy) that are sealed with a custom-made sample holder as in the case of de Jonge et al.¹⁹ The commercial devices require manual assembly and liquid supply through the sample holder. Evans et al. used the Hummingbird ScientificTM holder in a TEM to study lead sulfide nanoparticle growth.²⁹

Our group has used microfabrication technology to develop a nanofluidic liquid-cell (S)TEM device for *in situ* (S)TEM of fluid samples, dubbed the nanoaquarium.^{30,31} Figure 1a is a photograph (top view) and figure 1b is a three-dimensional schematic of the nanoaquarium. The nanoaquarium is made by direct bonding of silicon wafers coated with silicon nitride. One of the wafers also contains a thin film of patterned silicon oxide that

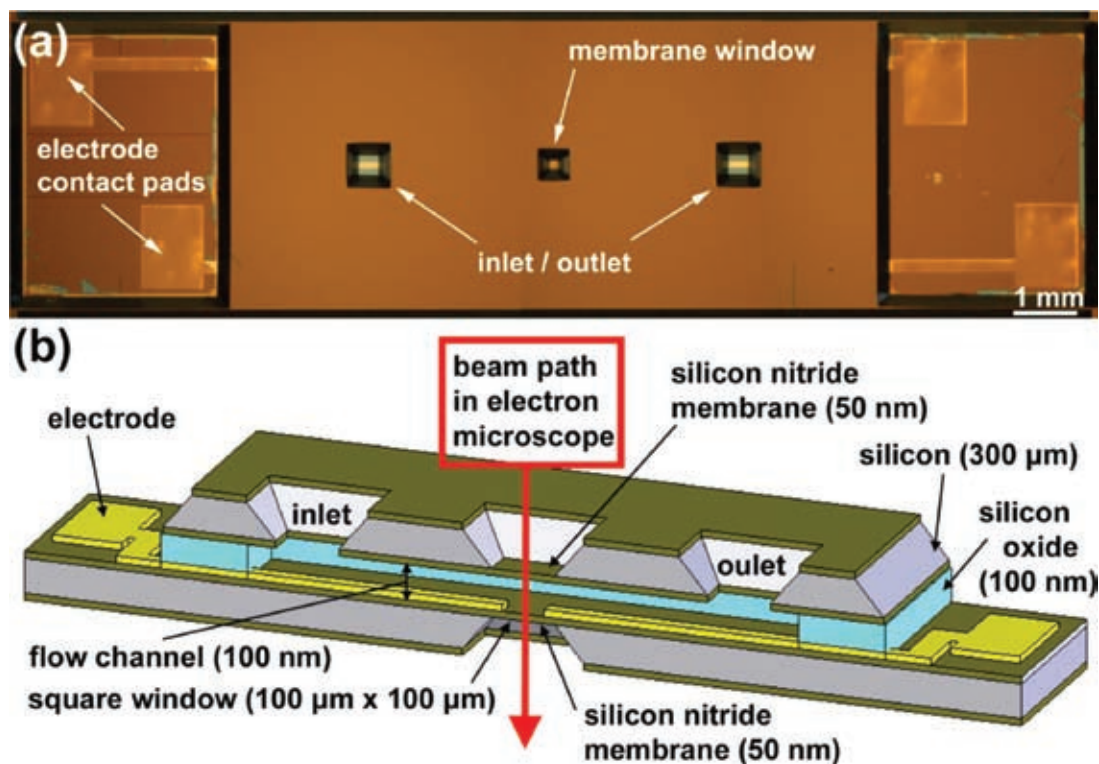


Figure 1: (a) Top view photograph of the nanoaquarium. (b) CAD illustration of the device sliced lengthwise down the center, showing the cross-section.

defines the geometry and height of the chamber and conduits. The thickness of the silicon oxide film, and thus the liquid cell's height, is controllable and can be prescribed to be tens to hundreds of nanometers. The first version of the nanoaquarium was made with a silicon oxide film that was 100 nm thick, and the imaging window was made of two 50 nm thick silicon nitride membranes. For the second version of the nanoaquarium, devices were produced with an oxide film that was up to 300 nm thick. The device fits into a custom-made holder and can sustain the high vacuum environment of the electron microscope for many hours without any noticeable loss of liquid. Some of the nanoaquarium's highlights include:

- An exceptionally thin sample cross-section, which translates to improved contrast and resolution. The technique can be used to produce channels and chambers as thin as a few tens of nanometers. The chamber spacing on each device is highly controllable thanks to the wafer bonding process. When preparing the device for imaging, there is no risk of debris incorporation that could modify the height of the chamber, which is a concern in other individually assembled devices.
- Wafer scale processing that enables high yield mass production, as opposed to production on a device-by-device basis.
- Robust hermetic sealing that provides leak-free operation without the use of glues, epoxies, or polymer spacers. These materials are a potential source of contamination and/or device failure. When the nanoaquarium is filled with a solution, the only materials in contact with the solution are silicon, silicon nitride, and silicon oxide (as well as titanium and platinum or gold when the optional electrodes are present). At the inlet and outlet, the solution is also in contact with O-rings; however, the inlet and outlet are far from the imaging window and robust, chemically inert material can be selected for the O-rings such that there is no threat of contamination. This makes the nanoaquarium uniquely suited to handle harsh chemistries such as strong solvents, acids, or bases.
- Compatibility with lab-on-chip technology, which, among other things, allows one to incorporate into the device liquid storage chambers, pumps and stirrers to control and manipulate liquids and reagents, as well as optical waveguides.
- On-chip integrated electrodes for sensing and actuation due to the use of a dielectric material as the spacer.
- The nanoaquarium can be used in either a static mode without flow, or a continuous flow mode. In static mode, the nanoaquarium is self-contained and does not require fluidic feed-through in the sample holder. This simplifies construction, reduces the cost of the sample holder and minimizes the volume of solution consumed in an experiment.
- The nanoaquarium can be made to include pillars that connect the top membrane to the bottom membrane in the window region to mitigate the problem of membranes bowing out in the vacuum environment.
- The nanoaquarium is intended to be used as a disposable device to avoid cross-contamination; however, devices can be reused when desired. The nanoaquarium can be removed from the holder, drained, and refilled with a new/fresh solution as needed for the experiment.

3 Nanoaquarium Fabrication Method

The nanoaquarium is fabricated with standard microfabrication techniques. For a detailed description of the fabrication process, see Grogan and Bau.³⁰ In this section, we describe the fabrication process only briefly. Figure 2 depicts the various fabrication steps. The fabrication process starts with prime grade, double-sided polished, Si wafers with <100> orientation. We deposit stoichiometric silicon nitride (~50 nm) by low pressure chemical vapor deposition on all surfaces of the wafers. The thickness of the SiN determines the thickness of the membrane windows that sandwich the liquid-filled imaging chamber and enable electron transmission. 50 nm SiN windows allow resolution of <0.2 nm at 200 kV.³² When and if desired, the windows can be made even thinner.

Two mating wafers are used to construct the top and bottom of the nanoaquarium. When electrodes (or heaters) are desired, we deposit an adhesion layer and pattern platinum electrodes and/or heaters on the bottom wafer's topside by lift-off technique. Next, we overlay silicon oxide by plasma-enhanced chemical vapor deposition and polish the oxide coating with a chemical-mechanical polisher. The thickness of the silicon oxide layer determines the height of the imaging chamber and the path length of the electrons. The silicon oxide also insulates the metallic paths from the fluid chamber. The silicon oxide is densified and degassed by heating the wafer in a vacuum oven at 300°C–500°C for several hours. This treatment prevents excessive outgassing from the silicon oxide during subsequent bond annealing, which otherwise might cause separation of bonded wafers.

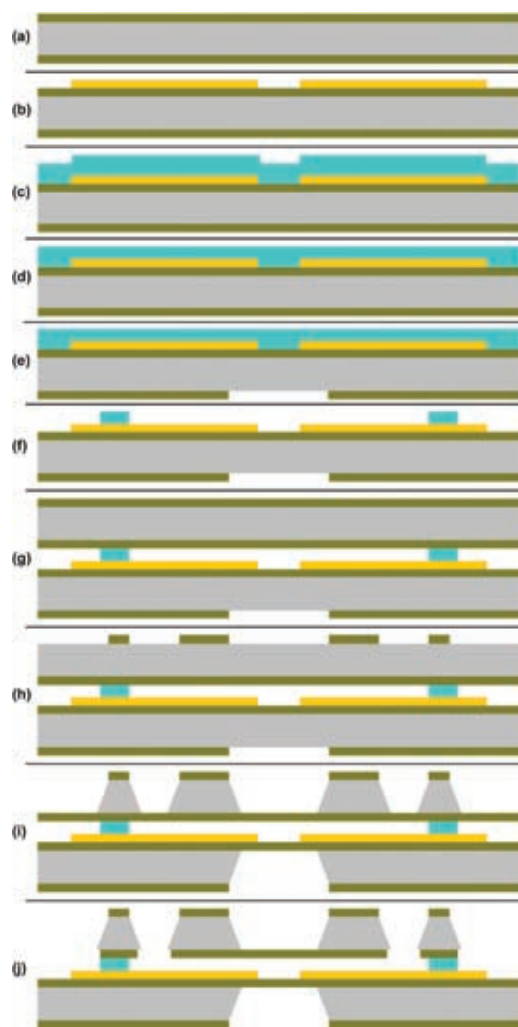


Figure 2: Depiction of the various fabrication steps. Color coded as follows: gray—silicon, green—silicon nitride, yellow—electrode stack, blue—silicon oxide. (a) 50 nm silicon nitride deposited by LPCVD. (b) 30 nm Ti/Au or Pt/Ti electrode stack deposited and patterned by evaporation and lift-off. (c) 150 nm–450 nm silicon oxide deposited by PECVD. (d) Oxide planarization in a CMP. (e) Backside nitride patterned in RIE. (f) Frontside oxide patterned with BOE. (g) Plasma activated wafer bonding to a blank nitride-coated wafer. (h) Backside nitride on top wafer patterned in RIE. (i) Windows and vias etched with KOH. (j) Inlet, outlet, and electrodes are exposed.

Next, we pattern the silicon oxide layer using buffered oxide etch to define the imaging chamber(s) and conduits, and to expose the electrodes at desired locations. The imaging chamber contains pillars to connect the chamber's floor to its ceiling to minimize bowing of the thin SiN windows when the device is inserted in the vacuum chamber of the electron microscope. We then pattern the nitride on the back side of the

bottom wafer in a reactive ion etcher to form the observation window pattern. Then, we thoroughly clean both the patterned and unpatterned wafers with piranha solution (sulfuric acid and hydrogen peroxide) and RCA1 (ammonium hydroxide, hydrogen peroxide, and water); plasma activate the surfaces to be bonded; and bond the bottom, patterned wafer directly to the top, unpatterned one. The bonded wafers are annealed at 250°C for 2–4 hours. Next, we pattern the nitride on the upper side of the top (blank) wafer in a reactive ion etcher so that the observation windows on the top and bottom wafers are aligned. Using the patterned silicon nitride as a mask, we etch the bonded wafer stack in potassium hydroxide solution to define the inlets, outlets, imaging windows, and access to metal pads. Many devices are fabricated concurrently on a single silicon wafer (Figure 3). The individual chips are separated and any remaining nitride in the inlets and outlets and above the electrode pads is removed (Figure 1).

4 Experiments with the Nanoaquarium

We have demonstrated the usefulness of the nanoaquarium for studying a variety of phenomena such as interactions among nanocrystals, aggregation of nanoparticles, interactions between nanoparticles and contact lines, and electrochemical processes.

4.1 Interactions between nanoparticles

Colloidal crystals (or metamaterials) are formed by oriented assembly of particles. The nanoaquarium is well suited to image interactions among nanoparticles. Figure 4 shows a pair of video frames, taken one second apart, of 50 nm diameter gold particles suspended in water. The images were taken in a STEM (FEI Quanta 600 FEG Mark II) with 20 kV acceleration voltage. The left frame features a cluster of two particles (a dimer) which is subsequently joined by a third particle in the right frame to form a trimer. The 50 nm gold particles provide high contrast and can be seen very clearly with a relatively low voltage electron beam. Similar experiments can also be used to examine the assembly of anisotropic particles and monitor orientational adjustments during aggregation.

4.2 Diffusion-limited aggregation

One of our early investigations was on diffusion limited aggregation of 5 nm gold particles suspended in water.³¹ Although the phenomenon is now well understood, most of the information on the details of the aggregation process were obtained through computational experiments. The nanoaquarium experiment is perhaps the

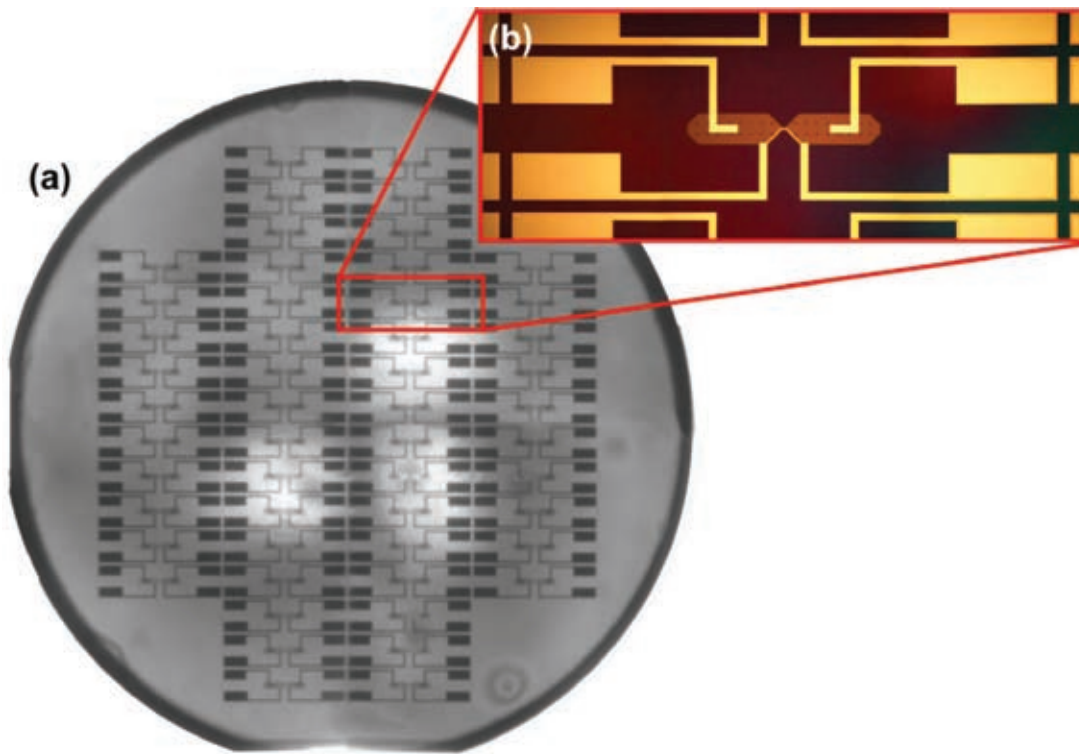


Figure 3: (a) An infrared image of a bonded pair of wafers with embedded devices showing excellent void-free bonding. Each set of bonded wafers contains 52 devices. (b) Zoomed in photo of the patterned bottom wafer prior to bonding.

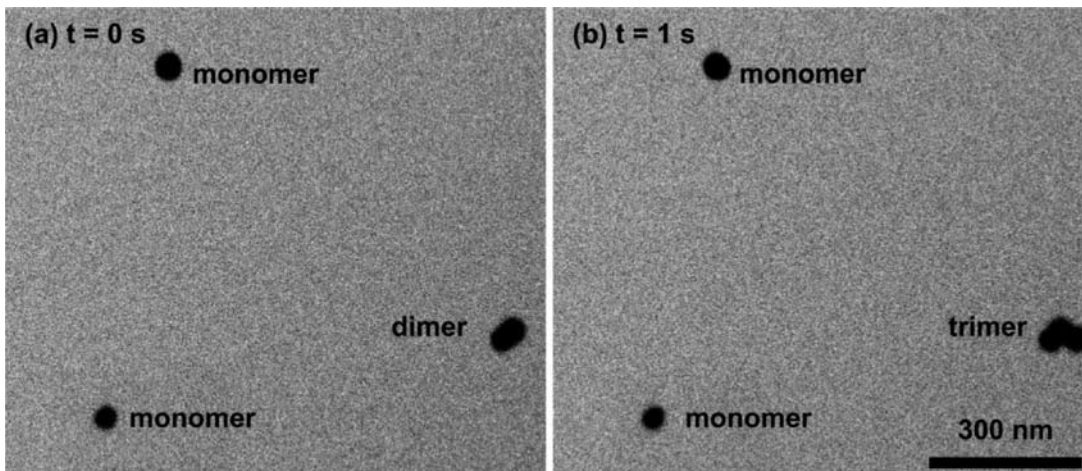


Figure 4: STEM images of 50 nm gold colloids in water showing the interactions of individual particles and small clusters. The dimer in the left frame becomes a trimer in the right frame by the addition of a monomer that entered from outside the field of view.

only study that has provided detailed dynamic information at the single particle level. The suspension was drawn into the nanoaquarium by surface tension forces, and imaging was performed at 20–30 kV in a STEM (FEI Quanta 600 FEG Mark II). Figure 5 features a few video frames, spaced 28 seconds apart, taken during the

aggregation process. A sample video is available at <http://arxiv.org/abs/1010.3286>. Among other phenomena, the videos enabled us to monitor the growth rate of clusters and image interactions among clusters. For example, figure 6 depicts the average number of nanoparticles in a cluster as a function of time. The symbols and the solid line

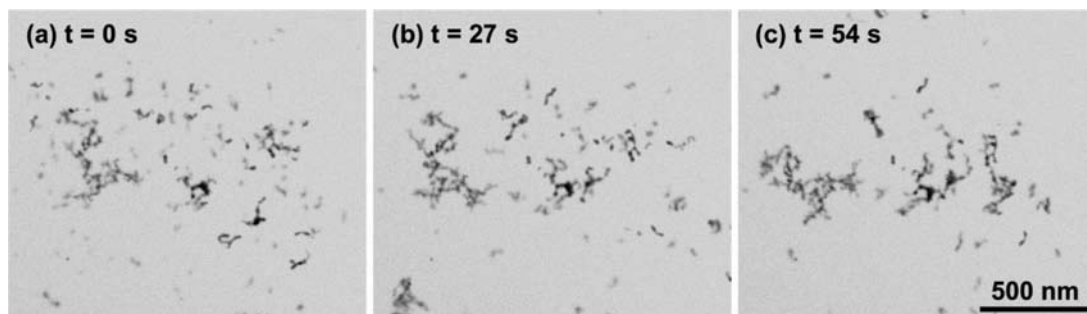


Figure 5: Aggregating nanoparticles. Three frames from recorded video of 5 nm gold particles and clusters composed thereof, as observed *in situ* with STEM.

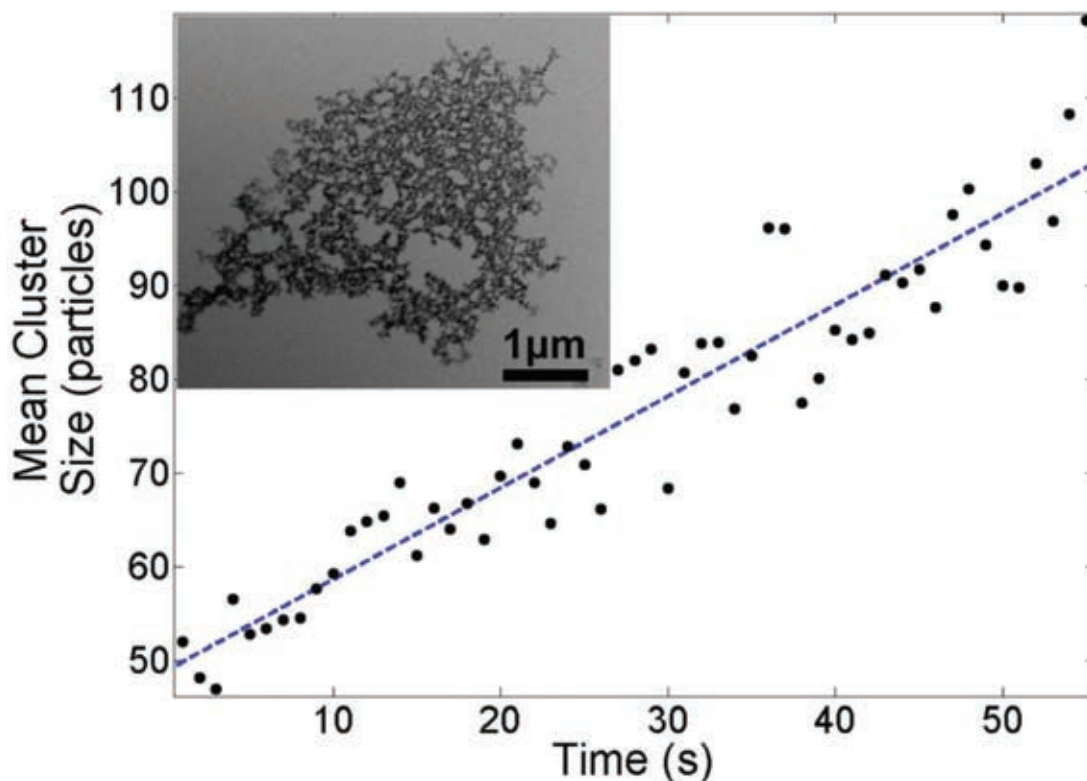


Figure 6: The average number of nanoparticles in a cluster is shown as a function of time for the growth process pictured in Figure 5. The symbols and dashed line correspond, respectively, to experimental data and theoretical predictions. Inset shows a large aggregate grown in the same system for a long time. The fractal dimension of the cluster, $D_f \sim 1.77$, measured using FracLac for ImageJ, is consistent with three-dimensional cluster-cluster diffusion-limited aggregation. Fractal dimension describes the exponential scaling relation between physical size and mass or complexity of a structure.

correspond, respectively, to experimental data and theoretical predictions. The experimental data is consistent with the predicted linear growth. The process results in the formation of the fractal structure shown in the inset.

Some of the regions of the imaging window (Figure 5) featured small clusters of particles in the process of aggregating, and others contained sizable aggregates. While the height of the

nanochannel limited the height of the aggregates to less than 300 nm, the projected area of many of these large aggregates exceeded several microns. And yet the fractal dimension of the large aggregates (about 1.77) was consistent with 3-D cluster-cluster diffusion-limited aggregation. Indeed, it seems odd that relatively large clusters would exhibit characteristics of three-dimensional growth when two-dimensional growth might be

expected due to confinement effects. The answer to this apparent paradox was revealed by observing the early stage aggregation, accessible with the nanoaquarium. We found that initially, clusters assemble in the channel from individual particles that are small relative to the conduit height, and they follow a three-dimensional growth habit. Eventually, the size of these growing clusters approaches the height of the channel and the clusters' movement is confined to a plane. Growth then proceeds through lateral cluster-cluster aggregation. Since these aggregating clusters already possess characteristics of growth in the three-dimensional regime, these characteristics are preserved in the resulting aggregate. Such insight would not have been possible without the capability to perform *in situ* observations on the aggregation process. Our experimental data agree with theoretical predictions for cluster growth and with experimental data obtained by other means, which suggests that the imaging technique has not altered the experiment in any significant way.

4.3 The interaction between nanoparticles and moving contact lines

Nanoscale investigation of the solid-liquid-vapor interface has remained a significant experimental challenge, but such studies are possible in the nanoaquarium.³³ The nanoaquarium was filled with an aqueous suspension of gold nanorods

(20 nm in diameter, 40 nm in length) stabilized with surfactant cetrimonium bromide (CTAB). Imaging was performed in a 30 kV STEM (FEI Quanta 600 FEG Mark II). Electrical potential of ~15 V was applied across the embedded electrodes to generate a bubble that displaced liquid (and nanorods) to the perimeter of the observation chamber. Figure 7 shows the vapor bubble surrounded by liquid. Witness the clear contrast between the low density (light color) vapor bubble and the higher density (dark color) liquid. We focused our observations at the interface between the bubble and the “bulk” liquid around the perimeter of the imaging window, which we refer to as the contact line. When the electron beam was focused onto the interface, the contact line moved (sometimes receding, sometimes advancing, and sometimes oscillating). At a receding contact line, nanorods were propelled away from the “bulk” liquid (opposite from the direction of contact line movement). See Figure 8 for the sequence of events. Interestingly, initially stationary particles did not move significantly until the contact line had passed by the particles by a distance of tens of nm. At an advancing contact line, nanorods were aligned and pushed into aggregates. Surprisingly, the initially stationary nanorods were not engulfed by the advancing contact line but were instead pushed ahead and formed a line that was parallel to the moving interface. Movies of these phenomena are available at <http://arxiv.org/abs/1110.3273>.

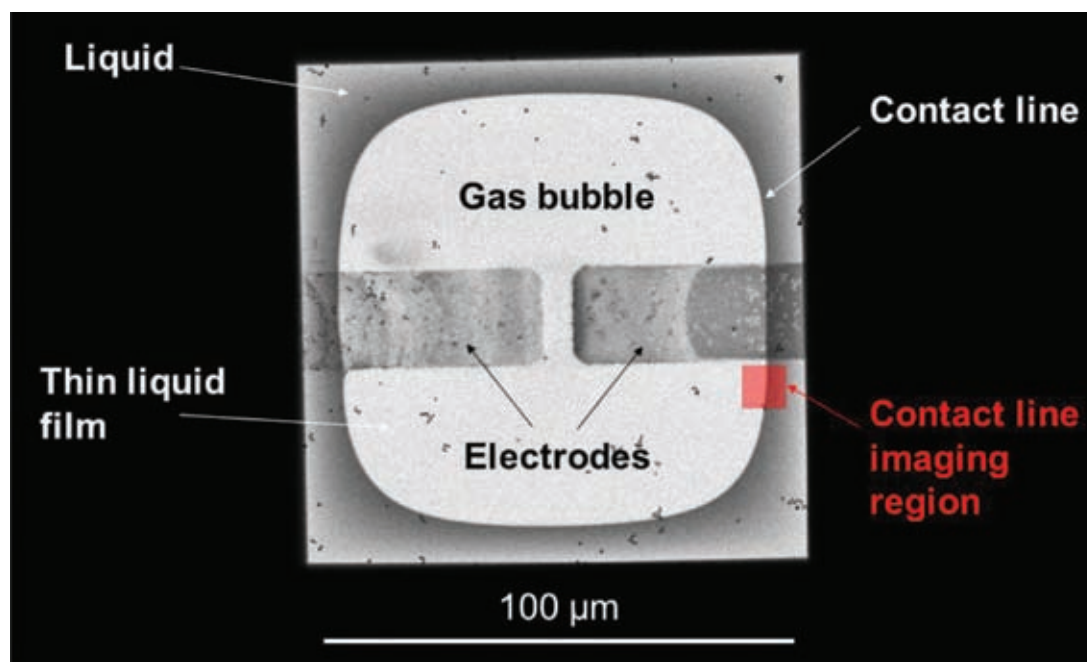


Figure 7: Top view STEM image of the nanoaquarium with a bubble (light gray) occupying most of the imaging window and liquid (dark gray) around the perimeter.

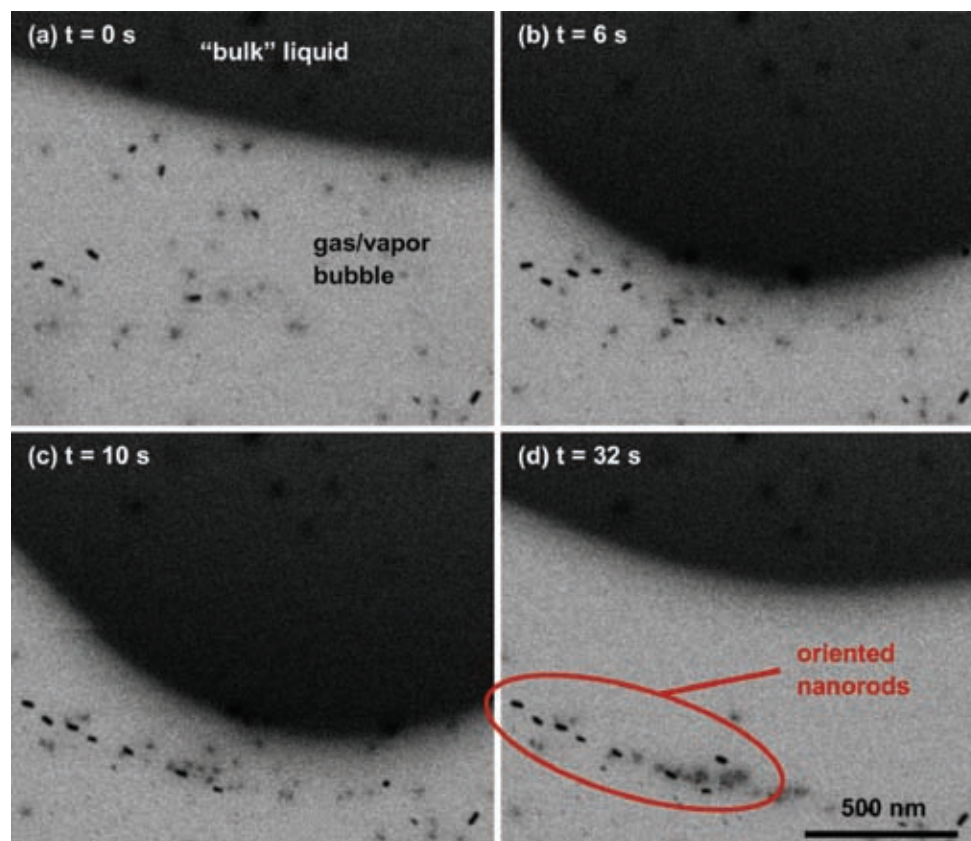


Figure 8: Orientation of gold nanorods under the influence of an advancing contact line. Note how initially scattered nanorods are pushed into alignment.

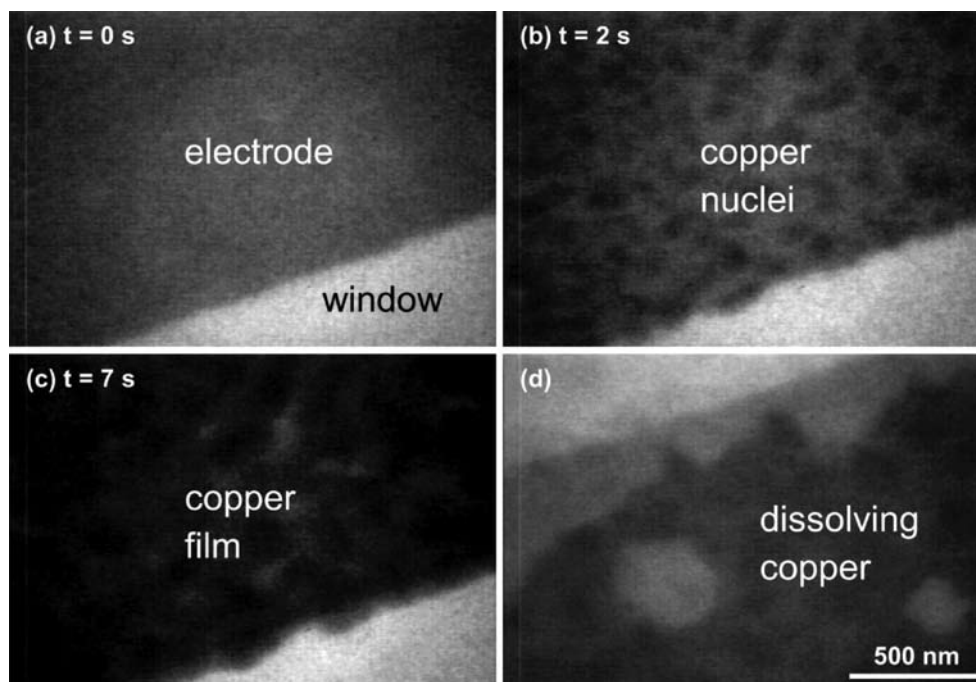


Figure 9: *In situ* TEM images of electrodeposition of copper on platinum electrodes from a solution of copper sulfate. (a)–(c) Potentiostatic deposition at -0.8 V relative to the open circuit potential. Time begins when potential is applied. (d) Potentiostatic stripping of the copper film at a different location on the electrode.

The experimental observations are consistent with a mathematical model that determines the fluid velocity in the thin film by considering the surface tension force and disjoining pressure in the thin liquid film.³⁴

4.4 Imaging of electrochemical processes

In situ electrochemistry is possible in the nanoaquarium by making use of the integrated electrodes. For example, deposition and stripping of copper in an acidified copper sulfate solution (0.1M CuSO_4 + 0.18M H_2SO_4) was performed in order to observe the onset of dendritic growth. Imaging was performed in a 300 kV TEM (Hitachi H9000) using a custom-made sample

holder with electrical connections. Deposition and stripping was performed through cyclic voltammetry and under potentiostatic conditions at a variety of potentials. At “low” voltage (−0.6 V relative to open circuit potential), sparse nucleation and growth of distinct clusters was observed. At “medium” voltage (−0.8 V relative to open circuit potential), dense nucleation that coalesced to form a continuous film was observed, along with some lateral growth beyond the electrode edge (Figure 9). At “high” voltage (−1.2 V relative to open circuit potential), rapid coverage of the electrode, followed by lateral growth of dendrites, was observed (Figure 10). These results extend the range of deposition conditions beyond those of prior work.^{15,16}

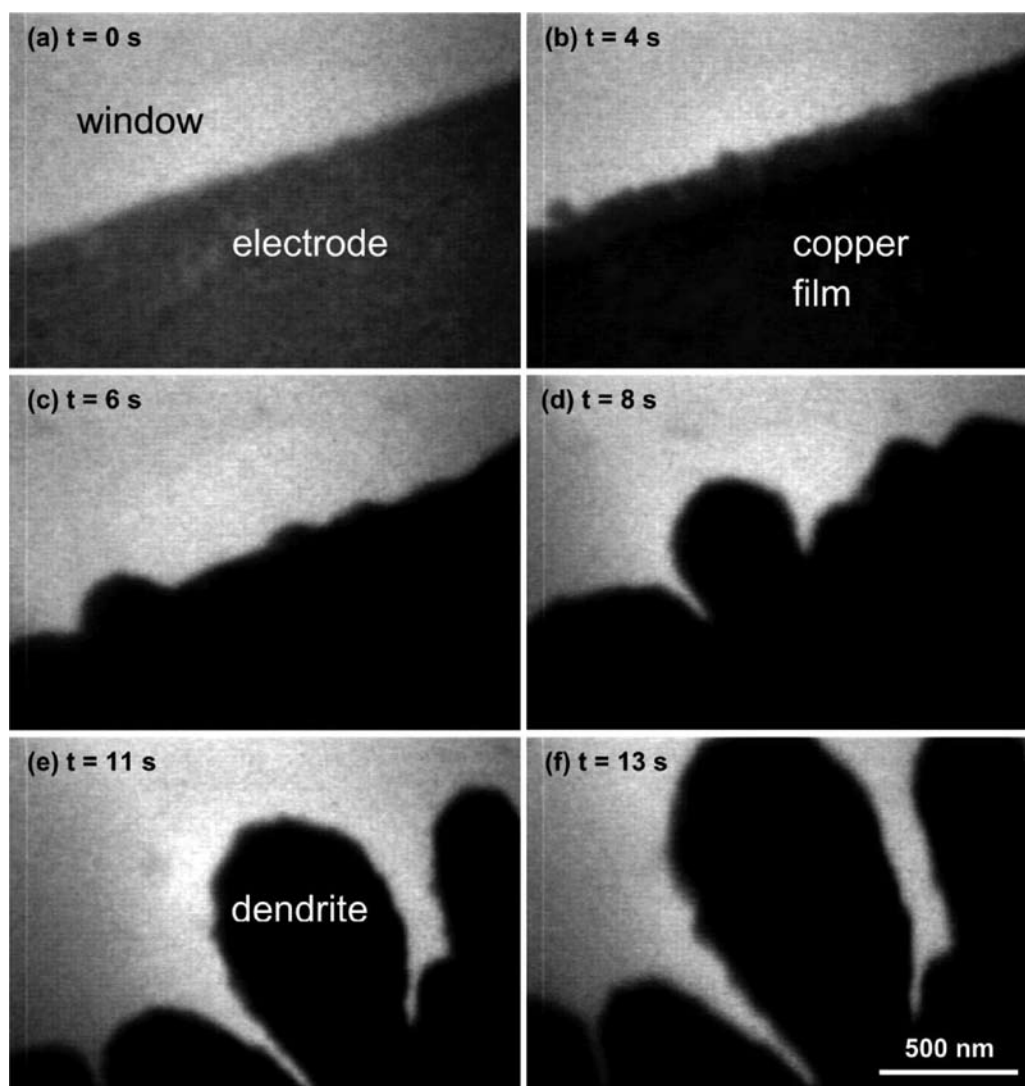


Figure 10: *In situ* TEM images of electrodeposition of copper on platinum electrodes from a solution of copper sulfate. (a)–(f) Potentiostatic deposition at −1.2 V relative to the open circuit potential. Time begins when potential is applied. Rapid coverage of the electrode followed by growth of dendrites is seen. The field of view moves upward throughout the series to track the growth.

5 Conclusions

We have described a new imaging tool, the nanoaquarium that allows researchers to image phenomena occurring in liquid media with the high resolution of the electron microscope. The utility of the device for studying oriented assembly, the formation of colloidal crystals, particle aggregation at interfaces, and electrochemical processes has been demonstrated. The nanoaquarium is likely to be useful in many other disciplines, in particular in biology, and to provide new insights into diverse processes.

The capabilities of the nanoaquarium can be greatly enhanced by enabling *in situ* manipulation and control of the processes being imaged. One can imagine processes taking place in laboratories-on-chips being imaged in real time. The potential of dynamic electron microscopy in liquid media is tremendous and is likely to lead to new insights and facilitate discoveries.

However, the electrons interact with the medium to be imaged in many ways, which are only partially understood. To image effectively processes taking place in liquid media, we must improve our understanding of the effects of electrons on liquids and the objects suspended in liquids.

Acknowledgments

The work was supported, in part, by grants #1066573 and #1129722 from the USA National Science Foundation (NSF) to the University of Pennsylvania. Fabrication was carried out at the Cornell NanoScale Facility, a member of the National Nanotechnology Infrastructure Network, which is supported by the National Science Foundation (Grant ECS-0335765). The facility staff graciously shared their wealth of expertise. Electron microscopy was performed at the Penn Regional Nanotechnology Facility, with the valuable assistance of Dr. Lolita Rotkina of the Penn Regional Nanotechnology Facility. Electron microscopy was also performed at the IBM T. J. Watson Research Center with the valuable assistance of Dr. Mark C. Reuter and Mr. Arthur Ellis of IBM. SumantSood of SUSS MicroTec shared expertise on wafer bonding. Peter Szczesniak of the MEAM Machine Shop at the University of Pennsylvania assisted in constructing the device holder. Dr. Brian Edwards (Department of Electrical & Systems Engineering, University of Pennsylvania) provided assistance with electromagnetic calculations. Professor Chris Murray (UPenn, Chemistry) generously provided encouragement and nanocrystals for our experiments.

Received 11 April 2012.

References

1. R. Erni, M. Rossell, C. Kisielowski, and U. Dahmen, "Atomic-Resolution Imaging with a Sub-50-pm Electron Probe," *Physical Review Letters*, vol. 102, no. 9, Mar. 2009.
2. G. Dannen, "Leo Szilard the Inventor." [Online]. Available: <http://www.dannen.com/budatalk.html>. [Accessed: 03-Apr-2012].
3. "Ernst Ruska—Autobiography." [Online]. Available: http://www.nobelprize.org/nobel_prizes/physics/laureates/1986/ruska-autobio.html. [Accessed: 03-Apr-2012].
4. P. G. de Gennes, "Wetting: statics and dynamics," *Reviews of Modern Physics*, vol. 57, pp. 827–863, 1985.
5. Y. A. Cengel and M. A. Boles, *Thermodynamics: An Engineering Approach*, 3rd ed. WCB/McGraw-Hill, 1998.
6. N. de Jonge and F. M. Ross, "Electron microscopy of specimens in liquid," *Nat Nano*, vol. 6, no. 11, pp. 695–704, Nov. 2011.
7. "How ESEM Works," *Imaging & Microscopy Facility, UC Merced*, Jun. 2003.
8. A. Bogner, G. Thollet, D. Basset, P. H. Jouneau, and C. Gauthier, "Wet STEM: A new development in environmental SEM for imaging nano-objects included in a liquid phase," *Ultramicroscopy*, vol. 104, no. 3–4, pp. 290–301, 2005.
9. I. Barshack, S. Polak-Charcon, V. Behar, A. Vainshtein, O. Zik, E. Ofek, M. Hadani, J. Kopolovic, and D. Nass, "Wet SEM: A Novel Method for Rapid Diagnosis of Brain Tumors," *Ultrastructural Pathology*, vol. 28, no. 4, pp. 255–260, Jul. 2004.
10. D. Joy and C. Joy, "Scanning electron microscope imaging in liquids—some data on electron interactions in water," *Journal of microscopy*, vol. 221, no. 2, pp. 84–88, 2006.
11. H. Sugi, "Electron Microscopic Visualization of the Cross-Bridge Movement Coupled with ATP Hydrolysis in Muscle Thick Filaments in Aqueous Solution, Reminiscences and Future Prospects," in *Muscle Biophysics*, vol. 682, Springer New York, 2010, pp. 77–103.
12. W. Timp and P. Matsudaira, "Chapter 14 Electron Microscopy of Hydrated Samples," in *Biophysical Tools for Biologists, Volume Two: In Vivo Techniques*, vol. 89, Academic Press, 2008, pp. 391–407.
13. W. Timp, N. Watson, A. Sabban, O. Zik, and P. Matsudaira, "Wet electron microscopy with quantum dots," *BioTechniques*, vol. 41, no. 3, pp. 295–298, Sep. 2006.
14. M. Krueger, S. Berg, D. A. Stone, E. Strelcov, D. A. Dikin, J. Kim, L. J. Cote, J. Huang, and A. Kolmakov, "Drop Casted Self Assembling Graphene Oxide Membranes for Scanning Electron Microscopy on Wet and Dense Gaseous Samples," *ACS nano*, 2011.
15. M. J. Williamson, R. M. Tromp, P. M. Vereecken, R. Hull, and F. M. Ross, "Dynamic microscopy of nanoscale cluster growth at the solid-liquid interface," *Nat Mater*, vol. 2, no. 8, pp. 532–536, 2003.
16. A. Radisic, P. M. Vereecken, J. B. Hannon, P. C. Searson, and F. M. Ross, "Quantifying Electrochemical Nucleation and Growth of Nanoscale Clusters Using Real-Time

- Kinetic Data,” *Nano Letters*, vol. 6, no. 2, pp. 238–242, Feb. 2006.
17. A. Radisic, P. M. Vereecken, P. C. Searson, and F. M. Ross, “The morphology and nucleation kinetics of copper islands during electrodeposition,” *Surface Science*, vol. 600, no. 9, pp. 1817–1826, May 2006.
 18. K.-L. Liu, C.-C. Wu, Y.-J. Huang, H.-L. Peng, H.-Y. Chang, P. Chang, L. Hsu, and T.-R. Yew, “Novel microchip for in situ TEM imaging of living organisms and bio-reactions in aqueous conditions,” *Lab Chip*, vol. 8, no. 11, pp. 1915–1921, 2008.
 19. N. de Jonge, D. B. Peckys, G. J. Kremers, and D. W. Piston, “Electron microscopy of whole cells in liquid with nanometer resolution,” *Proceedings of the National Academy of Sciences*, vol. 106, no. 7, pp. 2159–2164, Feb. 2009.
 20. D. B. Peckys, G. M. Veith, D. C. Joy, and N. de Jonge, “Nanoscale Imaging of Whole Cells Using a Liquid Enclosure and a Scanning Transmission Electron Microscope,” *PLoS ONE*, vol. 4, no. 12, p. e8214, Dec. 2009.
 21. E. A. Ring and N. de Jonge, “Microfluidic System for Transmission Electron Microscopy,” *Microscopy and Microanalysis*, pp. 1–8, 2010.
 22. N. de Jonge, N. Poirier-Demers, H. Demers, D. B. Peckys, and D. Drouin, “Nanometer-resolution electron microscopy through micrometers-thick water layers,” *Ultramicroscopy*, vol. 110, no. 9, pp. 1114–1119, Aug. 2010.
 23. H. Zheng, S. A. Claridge, A. M. Minor, A. P. Alivisatos, and U. Dahmen, “Nanocrystal Diffusion in a Liquid Thin Film Observed by in Situ Transmission Electron Microscopy,” *Nano Letters*, vol. 9, no. 6, pp. 2460–2465, Jun. 2009.
 24. H. Zheng, R. K. Smith, Y. Jun, C. Kisielowski, U. Dahmen, and A. P. Alivisatos, “Observation of Single Colloidal Platinum Nanocrystal Growth Trajectories,” *Science*, vol. 324, no. 5932, pp. 1309–1312, Jun. 2009.
 25. E. R. White, M. Mecklenburg, S. B. Singer, S. Aloni, and B. C. Regan, “Imaging Nanobubbles in Water with Scanning Transmission Electron Microscopy,” *Applied Physics Express*, vol. 4, no. 5, p. 055201, Apr. 2011.
 26. J. F. Creemer, S. Helveg, G. H. Hoveling, S. Ullmann, A. M. Molenbroek, P. M. Sarro, and H. W. Zandbergen, “Atomic-scale electron microscopy at ambient pressure,” *Ultramicroscopy*, vol. 108, no. 9, pp. 993–998, Aug. 2008.
 27. J. F. Creemer, S. Helveg, P. J. Kooyman, A. M. Molenbroek, H. W. Zandbergen, and P. M. Sarro, “A MEMS Reactor for Atomic-Scale Microscopy of Nanomaterials Under Industrially Relevant Conditions,” *J. Microelectromech. Syst.*, vol. 19, no. 2, pp. 254–264, Apr. 2010.
 28. L. Mele, F. Santagata, G. Pandraud, B. Morana, F. D. Tichelaar, J. F. Creemer, and P. M. Sarro, “Wafer-level assembly and sealing of a MEMS nanoreactor for in situ microscopy,” *Journal of Micromechanics and Microengineering*, vol. 20, p. 085040, 2010.
 29. J. E. Evans, K. L. Jungjohann, N. D. Browning, and I. Arslan, “Controlled Growth of Nanoparticles from Solution with In Situ Liquid Transmission Electron Microscopy,” *Nano Lett.*, vol. 11, no. 7, pp. 2809–2813, 2011.
 30. J. M. Grogan and H. H. Bau, “The Nanoaquarium: A Platform for In Situ Transmission Electron Microscopy in Liquid Media,” *Journal of Microelectromechanical Systems*, vol. 19, no. 4, pp. 885–894, 2010.
 31. J. M. Grogan, L. Rotkina, and H. H. Bau, “In situ liquid-cell electron microscopy of colloid aggregation and growth dynamics,” *Phys. Rev. E*, vol. 83, no. 6, Jun. 2011.
 32. R. Ramachandra, H. Demers, and N. de Jonge, “Atomic-resolution scanning transmission electron microscopy through 50-nm-thick silicon nitride membranes,” *Applied Physics Letters*, vol. 98, no. 9, p. 093109, 2011.
 33. J. M. Grogan and H. H. Bau, “Real Time Electron Microscope Imaging of Nanoparticle Motion Induced by a Moving Contact Line,” *arXiv.org*, 2011.
 34. J. M. Grogan, “The Nanoaquarium: A Nanofluidic Platform for in situ Transmission Electron Microscopy in Liquid media,” Ph.D. Dissertation, University of Pennsylvania, Philadelphia, PA, USA, 2011.



Joseph M. Grogan received the B.E. degree with high honors in Mechanical Engineering from Stevens Institute of Technology, Hoboken, NJ, USA in 2004 and Ph.D. degree in Mechanical Engineering and Applied Mechanics from the University of Pennsylvania, Philadelphia, PA, USA in 2011. He is currently a post-doctoral researcher at the University of Pennsylvania. His research interests include micro and nanofluidics, in situ electron microscopy, micro and nanofabrication techniques, and radiation chemistry. Dr. Grogan is a member of the Microscopy Society of America.



Nicholas M. Schneider is a Ph.D. student working with Dr. Haim H. Bau at the University of Pennsylvania in Mechanical Engineering and Applied Mechanics. Nicholas received concurrent B.S. and M.S. degrees from Rochester Institute of Technology, Rochester, NY, in 2010. His research focuses on *in situ* electron microscopy in liquids of biological and colloidal systems.



Frances M. Ross received her B.A. and Ph.D. degrees from the University of Cambridge, UK. After post-doctoral research at AT&T Bell Laboratories, she worked at the National Center for Electron Microscopy at the Lawrence Berkeley National Laboratory, Berkeley, CA, USA, then joined the IBM T.J. Watson Research Center as a Research Staff Member. She has authored or co-authored over 100 journal articles and 7 patents, and is a Fellow of APS, MRS, MSA and the UK Institute of Physics. Her interests include crystal growth physics and in situ microscopy techniques.



Haim H. Bau received the B.S. degree in Mechanical Engineering from Technion – Israel Institute of Technology, Haifa, Israel in 1969 and Ph.D. degree in Mechanical Engineering from Cornell University, Ithaca, NY, USA in 1980. He is a Professor of Mechanical Engineering and Applied Mechanics at the University of Pennsylvania, Philadelphia, PA. He has authored or co-authored over 128 archival journal papers and numerous conference proceeding papers. Professor Bau is a Fellow of ASME.